



DNA strand breaks based on Monte Carlo simulation in and around the Lipiodol with flattening filter and flattening filter-free photon beams

Daisuke Kawahara¹, Akito Saito¹, Hisashi Nakano², Yasushi Nagata¹

¹Department of Radiation Oncology, Institute of Biomedical and Health Sciences, Hiroshima University, Hiroshima, Japan

²Department of Radiation Oncology, Niigata University Medical and Dental Hospital, Niigata, Japan

ABSTRACT

Background: The current study aims to investigate the DNA strand breaks based on the Monte Carlo simulation within and around the Lipiodol with flattening filter (FF) and flattening filter-free (FFF) photon beams.

Materials and methods: The dose-mean lineal energy (y_D) and DNA single- and double strand breaks (DSB/SSB) based on spatial patterns of inelastic interactions were calculated using the Monte Carlo code: particle and heavy ion transport system (PHITS). The ratios of dose using standard radiation (200 kVX) to the dose of test radiation (FF and FFF of 6 MV X-ray (6MVX) and 10 MVX beams) to produce the same biological effects was defined as RBE_{DSB} . The RBE_{DSB} within the Lipiodol and in the build-up and build-down regions was evaluated.

Results: The RBE_{DSB} values with the Lipiodol was larger than that without the Lipiodol at the depth of 4.9 cm by 4.2% and 2.5% for 6 MVX FFF and FF beams, and 3.3% and 2.5% for 10 MVX FFF and FF beams. The RBE_{DSB} values with the Lipiodol was larger than that without the Lipiodol at the depth of 6.5 cm by 2.9% and 2.4% for 6 MVX FFF and FF beams, and 1.9% and 1.4% for 10 MVX FFF and FF beams. In the build-down region at the depth of 8.1 cm, the RBE_{DSB} values with the Lipiodol was smaller than that without the Lipiodol by 4.2% and 2.9% for 6 MVX FFF and FF beams, and 1.4% and 0.1% for 10 MVX FFF and FF beams.

Conclusions: The current study simulated the DNA strand break except for the physical dose difference. The lower and FFF beam occurred the higher biological effect.

Key words: build-up; build-down; Lipiodol; double strand breaks; Monte Carlo

Rep Pract Oncol Radiother 2022;27(3):392-400

Introduction

DNA damage by irradiation may lead to cell death. Theoretical calculation approaches complement experimental research on the induction of DNA damage under various conditions. It can simulate the DNA damage by various irradiation conditions quantitatively [1]. Irradiation with photon beam on tissue causes the generation of secondary electrons due to various interactions such as

photoelectric absorption and Compton scattering [2]. DNA damage leading to cell death and chromosomal aberrations is caused by the energies of secondary electrons deposited into cells [3]. The biological effectiveness (RBE) can be evaluated by analyzing the local energy deposition of secondary electrons on micro- or nano-meter scale [4].

Previously, Monte Carlo (MC) simulation codes such as PARTRAC, Geant4-DNA, and KURBUC have been used to evaluate the DNA damage

Address for correspondence: Daisuke Kawahara, Department of Radiation Oncology, Institute of Biomedical and Health Sciences, Hiroshima University, 1-2-3 Kasumi, Minami-ku, Hiroshima-shi, Hiroshima 734-8551, Japan; e-mail: daika99@hiroshima-u.ac.jp

This article is available in open access under Creative Common Attribution-Non-Commercial-No Derivatives 4.0 International (CC BY-NC-ND 4.0) license, allowing to download articles and share them with others as long as they credit the authors and the publisher, but without permission to change them in any way or use them commercially

by irradiation [5–7]. PARTRAC and KURBUC are based on electron scattering cross sections in water vapor, and Geant-DNA is based on a combination of analytical and interpolated cross sections for liquid water. However, these remain uncertain of the quality of radiation transport at the lower energy below sub-kiloelectron volt. On the other hand, Particle and Heavy Ion Transport code System (PHITS) can simulate the track structure of electrons in liquid water in the low energy range below sub-kilo electron volt [8–10]. The biological effect has been generally investigated with the RBE based on the linear–quadratic (LQ) model [11, 12]. However, the β that is a parameter of the survival fraction calculation based on the LQ model depends on the dose rate and cell lines as well as the profiles of radiation in a complicated manner [13]. Another study represented that the β is increasing with increasing LET [14]. Howkins et al. proposed a new model, Microdosimetric-kinetic (MK) model, which is able to predict the β value with increasing LET [15]. Our previous study showed the RBE enhancement within the Lipiodol with MK model [16]. The RBE according to the MK mode is calculated from dose and lineal energy ($yd(y)$). The dose mean lineal energy $d(y)$ is able to be obtained from PHITS simulation [17]. RBE was defined as the ratios of dose using reference radiation to the dose of test radiation to produce the same biological effects. However, the RBE defined in the previous study was affected by the physical dose in addition to the biological effect.

Recently, PHITS was updated, so that it can use the electron track structure mode (etsmode) [18]. It enables the evaluation of the impacts of low-energy electrons on the DNA strand break induction such as single strand break (SSB) and double strand break (DSB) with Monte Carlo simulation. Namely, it can evaluate the biological effect directly.

A previous study evaluated the dose enhancement within the Lipiodol (Guerbet, Villepinte, France) which includes a high-atomic number material [19]. Lipiodol has been used as an embolic agent in trans-arterial chemoembolization (TACE). The dose enhancement is larger with FFF beam than that with FF beam [20]. Also, we investigated the dose difference with and without the Lipiodol in the build-up region [21]. The area of the dose enhancement by the backscatter was within 3 mm from the Lipiodol. Other studies reported the dosimetric effects in the build-up

and build-down regions for the high-atomic number materials such as the metal material [22, 23]. However, these dose differences were calculated with the physical dose. Thus, the factor for the difference of the DNA damage with and without the Lipiodol was not revealed.

In the current study, the DNA stand breaks and the RBE calculated using the ratio of DNA-DSBs were evaluated in and around the Lipiodol compared for FF and FFF of 6 MVX and 10 MVX beam, except for the physical dose difference.

Materials and methods

Monte Carlo calculations

A TrueBeam linac (Varian Medical Systems, Palo Alto, USA) for FF and FFF of 6 MVX and 10 MVX beams was modelled. Varian provides IAEA-compliant phase-space files located just above the secondary X/Y collimator, which were simulated using the GEANT4 MC code. The IAEA-compliant phase-space was scored above the secondary collimator. The present study modelled the phase-space files below the secondary collimator using BEAMnrc [24]. The phase-space data scored at a source-to-surface distance (SSD) of 90 cm. In the Monte Carlo simulation, a Lipiodol ($3 \times 3 \times 3 \text{ cm}^3$) located at a depth of 5.0 cm in a virtual water-equivalent phantom ($30 \times 30 \times 30 \text{ cm}^3$) was modelled, as shown in Figure 1. Lipiodol includes an ethiodized oil injection and is a sterile injectable radio-opaque diagnostic agent. The Lipiodol in each millimeter contains 480 mg of iodine organically combined with ethyl esters of fatty acids of poppy seed oil [25]. The physical density and cross-section data were assigned for the Lipiodol and the water.

These phase-space files were transferred to the PHITS which is able to deal with the transport of nearly all particles such as protons, neutrons, electrons, and photons over a wide energy range [26]. The photon beams were irradiated with a $5 \times 5 \text{ cm}^2$ of field size at SSD = 90 cm for the virtual phantom.

The dose-mean lineal energy (y_D) is derived by [17]:

$$y_D = \frac{\int y^2 f(y) dy}{\int y f(y) dy} = \frac{\int y d(y) dy}{\int d(y) dy} \quad (1)$$

where $f(y)$ is the probability density of the lineal energy and $d(y)$ is the dose distribution of the lineal

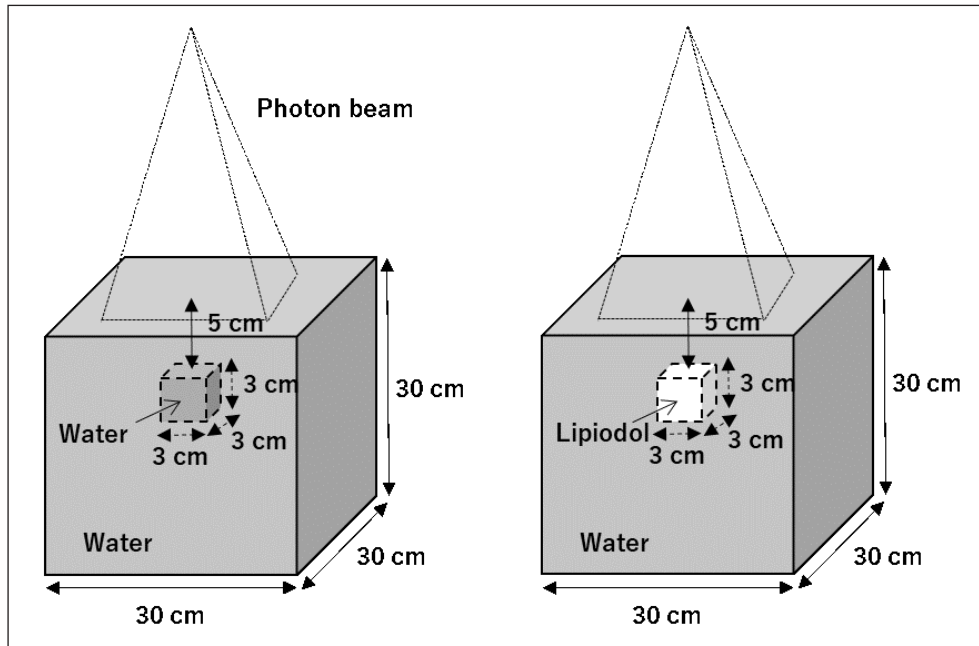


Figure 1. Geometric scheme of virtual water and Lipiodol located at a depth of 5.0 cm in a water-equivalent phantom (30 × 30 × 30 cm³)

energy. The energy spectrum and the dose-mean lineal energy within the Lipiodol, and in the build-up and build-down region were calculated.

Calculation of relative biological effectiveness

The yields of SSBs and DSBs were calculated with the track structure code which was incorporated in PHITS ver. 3.20. Through the medium, the electrons make much collisional positions. These sequential positions are defined as the track structure. Matsuya et al. reported that DSBs calculated using PHITS is in good agreement with the other simulation codes by Geant4-DNA and experimental data for both electron and photon irradiations [27]. The experimental DSB data was collected from the literature and performed a γ -H2AX focus formation assay [28–30]. Kai et al. showed the track structure is useful for the modeling of DNA damage [31]. In the track structure code in PHITS, the yields of SSBs and DSBs were calculated by stochastically sampling the number of events per track and that of a pair composed of two events within 3.4 nm (10 base pairs) [32]. It was based on the assumption that ionization and electronic excitation are potential causes to induce DNA strand breaks [33, 34]. The yield of SSBs and DSBs were calculated based on assuming that the number of

events per keV N_{event}/E_{in} and that of linkage per keV N_{event}/E_{in} are proportional to the induction yield of SSB and DSB.

$$Y_{SSB}(E_{in}) = k_{SSB} \frac{N_{event}}{E_{in}} \quad (2)$$

$$Y_{DSB}(E_{in}) = k_{DSB} \frac{N_{link}}{E_{in}} \quad (3)$$

The coefficients $k_{SSB} = 5.66 \times 10^{-12}$ (keV/Gy/Da) and $k_{DSB} = 1.61 \times 10^{-13}$ (keV/Gy/Da) were obtained by applying the PHITS to the experimental yields of SSB and DSB with 220 kVp X-rays [28].

The SSB and DSB, and the ratio of DSB and SSB (DSB/SSB) were calculated using the energy spectra of electrons after irradiation with FF and FFF of 6 MVX and 10 MVX beams on each grid within the Lipiodol and in the build-up and build-down regions. The build-up region was set at the 4.9 cm and build-down region was set at 8.1 cm.

Moreover, since the absorbed dose is related to the number of DNA-DSBs per nucleus [35], the ratio of DNA-DSBs for standard radiation of 200 kVp X-rays, which was defined as RBE_{DSB} , was calculated by:

$$RBE_{DSB} = \frac{DSB}{DSB_{200kVp X-rays}} \quad (4)$$

Table 1. The dosemean lineal energy in the water and Lipiodol for the flattening filter (FF) and flattening filter-free (FFF) of 6 MVX and 10 MVX beams within the Lipiodol and in the build-up and build-down regions

Region	6 MVX FF [keV/ μm]		6 MVX FFF [keV/ μm]		10 MVX FF [keV/ μm]		10 MVX FFF [keV/ μm]	
	Water	Lipiodol	Water	Lipiodol	Water	Lipiodol	Water	Lipiodol
Build-up	1.96	1.97	2.06	2.07	1.85	1.86	1.93	1.94
Within Lipiodol	1.97	2.05	2.08	2.17	1.86	1.93	1.93	2.00
Build-down	1.98	1.97	2.08	2.07	1.86	1.85	1.94	1.93

Results

The dose-mean lineal energy y_D

The dosemean lineal energy y_D values with and without the Lipiodol at 4.9 cm (build-up region), 6.5 cm (within the Lipiodol region), and 8.1 cm (build-down region) for the FF and FFF of 6 MVX and 10 MVX beams are shown in Table 1. The y_D values with the Lipiodol were larger than those without the Lipiodol by 0.5% for 6 MVX FF and 0.6% for 6 MVX FFF beams at the depth of 4.9 cm, and 3.9% with the Lipiodol and 4.6% without the Lipiodol at the depth of 6.5 cm for 6 MVX beam. For 10 MVX beam, the y_D values with the Lipiodol were larger than those without the Lipiodol by 0.3% for 10 MVX FF and 0.4% for 10 MVX FFF beams at the depth of 4.9 cm, and 3.5% for 10 MVX FF and 3.6% for 10 MVX FFF beams at the depth of 6.5 cm. On the other hand, the y_D values with the Lipiodol were smaller than those without the Lipiodol beam by -0.3% for 6 MVX FF and -0.4% for 6 MVX FFF beams at the depth of 4.9 cm in the build-down region. The y_D values with the Lipiodol for 10 MVX FFF beam were smaller than 10 MVX FF beam by -0.2% and -0.2% in the build-down region.

The yield of DSB/SSBs with and without Lipiodol

Figure 2 show the yield ratio of DSB/SSBs at 6.5 cm within the Lipiodol region and at 4.9 cm in the build-up and at 8.1 cm in the build-down regions for FF and FFF of 6 MVX and 10 MVX beams. The DSB/SSBs with the Lipiodol was larger than that without the Lipiodol by 2.5% for 6 MVX FF and 4.2% for 6 MVX FFF beams at the depth of 4.9 cm, and 2.4% with the Lipiodol and 2.9% without the Lipiodol at the depth of 6.5 cm. The DSB/SSBs and RBE_{DSB} with the Lipiodol were smaller than those without the Lipiodol by 2.9% for 6 MVX FF and 4.2% for 6 MVX FFF beams at the depth of

8.1 cm. Moreover, the RBE_{DSB} with the Lipiodol was larger than that without the Lipiodol by 2.5% for 10 MVX FF and 3.2% for 10 MVX FFF beams at the depth of 4.9 cm, and 1.4% with the Lipiodol and 1.9% without the Lipiodol at the depth of 6.5 cm. The RBE_{DSB} with the Lipiodol was smaller than that without the Lipiodol by 0.1% for 10 MVX FF and 1.2% for 10 MVX FFF beams at the depth of 8.1 cm.

The yield ratio of RBE_{DSB} with and without Lipiodol

Figure 3 shows the yield of and RBE_{DSB} at 6.5 cm within the Lipiodol region and at 4.9 cm in the build-up and at 8.1 cm in the build-down regions for FF and FFF of 6 MVX and 10 MVX beams. The yields of DSBs with the Lipiodol was larger than without the Lipiodol by 3.3% for 6 MVX FF beam and 3.7% for 6 MVX FFF beam at the depth of 4.9 cm, and 2.3% for 6 MVX FF beam and 2.7% for 6 MVX FFF beam at the depth of 6.5 cm. The yields of DSBs with the Lipiodol were smaller than those without the Lipiodol by 2.5% for 6 MVX FF beam and 4.0% for 6 MVX FFF beam at the depth of 8.1 cm. The yields of DSBs with the Lipiodol + were larger than those without the Lipiodol by 1.9% for 10 MVX FF beam and 3.2% for 10 MVX FFF beam at the depth of 4.9 cm, and 1.6% for 10 MVX FF beam and 1.7% for 10 MVX FFF beam at the depth of 6.5 cm. The yields of DSBs with the Lipiodol were smaller than those without the Lipiodol by 0.2% for 10 MVX FF beam and 1.4% for 10 MVX FFF beam at the depth of 8.1 cm.

For the comparison of the RBE_{DSB} with and without the Lipiodol, the DSB/SSBs and RBE_{DSB} with the Lipiodol were larger than those without the Lipiodol by 2.5% for 6 MVX FF and 4.2% for 6 MVX FFF beams at the depth of 4.9 cm, and 2.4% with the Lipiodol and 2.9% without the Lipiodol at the depth of 6.5 cm. The DSB/SSBs and RBE_{DSB} with the Lipiodol were smaller than those without

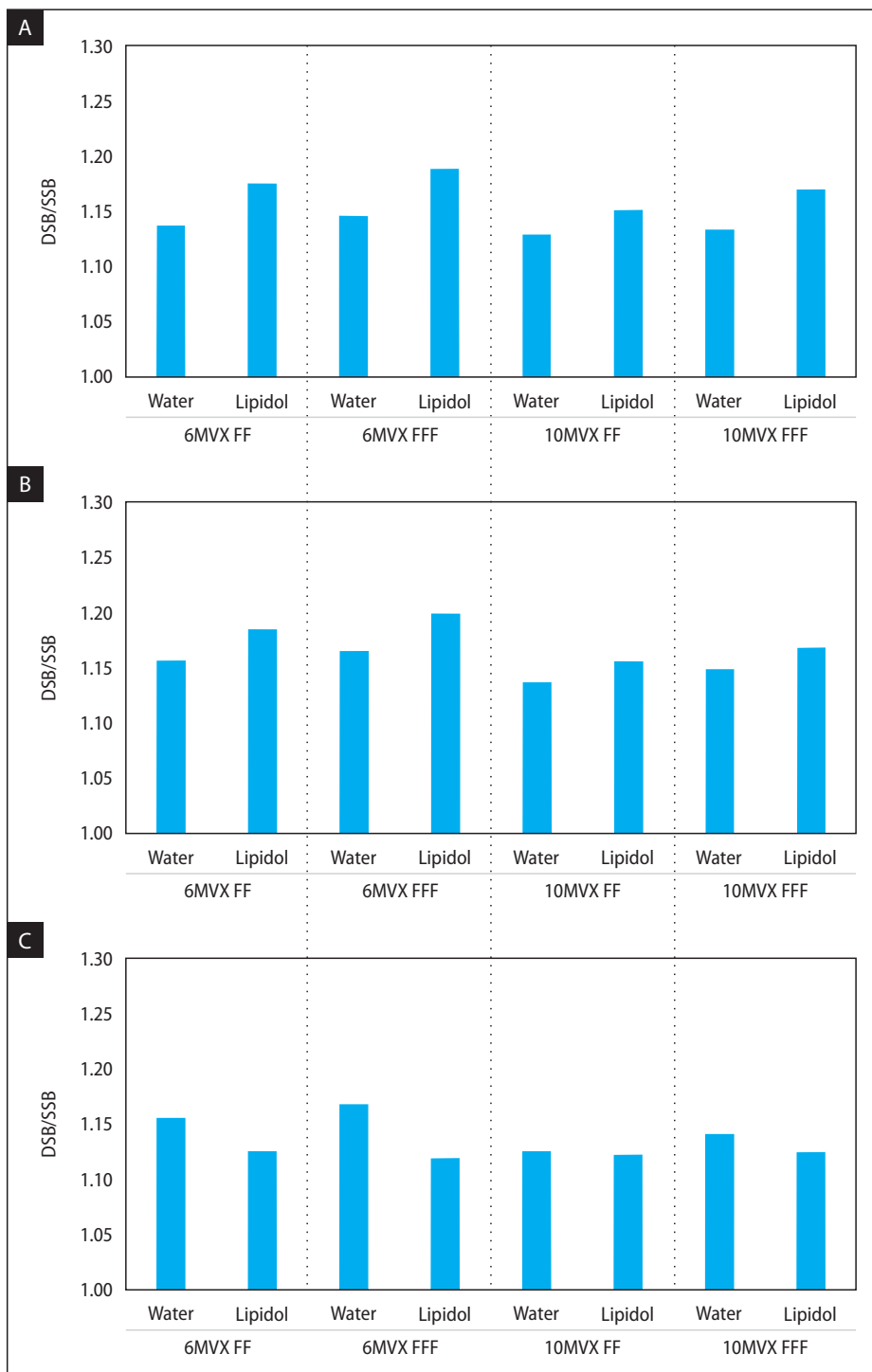


Figure 2. The yield ratio of single- and double strand breaks (DSB/SSB) with and without Lipidol for flattening filter (FF) and flattening filter-free (FFF) of 6 MVX and 10 MVX beams at the depth of 4.9 cm in the build-up region (A), 6.5 cm within the Lipidol (B), and 8.1 cm in the build-down region (C)

the Lipidol by 2.9% for 6 MVX FF and 4.2% for 6 MVX FFF beams at the depth of 8.1 cm. Moreover, the RBE_{DSB} with the Lipidol was larger than that without the Lipidol by 2.5% for 10 MVX FF and 3.3% for 10 MVX FFF beams at the depth of

4.9 cm, and 1.4% with the Lipidol and 1.9% without the Lipidol at the depth of 6.5 cm. The RBE_{DSB} with the Lipidol was smaller than that without the Lipidol by 0.1% for 10 MVX FF and 1.4% for 10 MVX FFF beams at the depth of 8.1 cm.

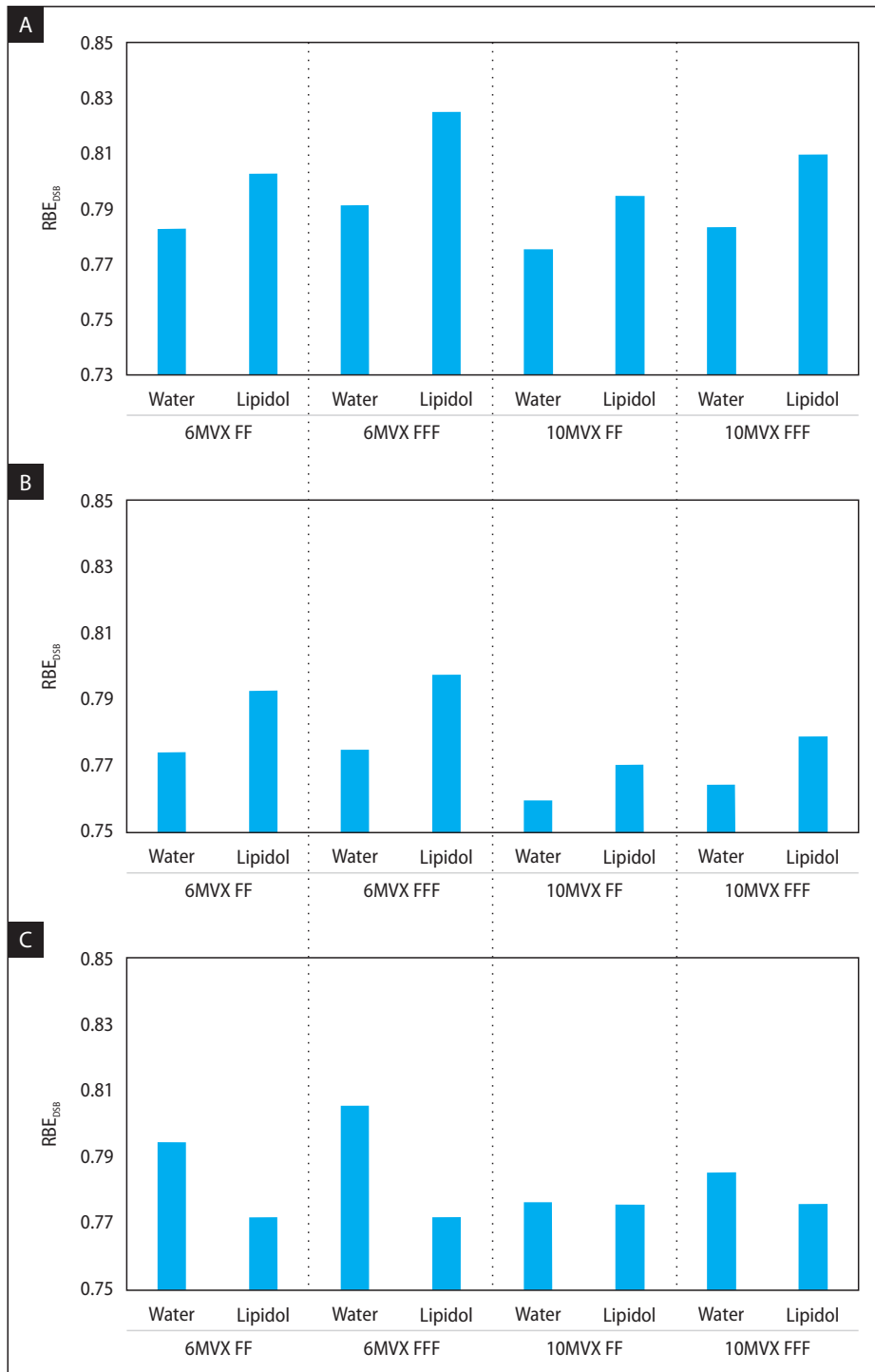


Figure 3 The RBE_{DSB} with and without Lipidol for flattening filter (FF) and flattening filter-free (FFF) of 6 MVX and 10 MVX beams at 4.9 cm in the build-up region (A), 6.5 cm within the Lipidol (B), and 8.1 cm in the build-down region (C)

Discussion

In this decades, high atomic number materials have attracted increasing attention as radiosensitizers. The physical dose enhancement has been investigated with the gadolinium, gold nano parti-

cle (GNP), and iodine [36–44]. The data of chemical and biological effect with the GNP was shown by Butterworth et al [45–47]. These experimental data represent that degree of radiosensitization is greater than the predicted increase in physical dose. A previous study investigated the biological dose

enhancement with and without the Lipiodol [16]. We indicated a possibility of the enhancement of the biological effect by the result that the biological dose enhancement was higher than the physical dose enhancement. However, the biological dose included the physical dose and the biological effect. The current study investigated the DNA strand breaks except for the physical dose difference with and without the Lipiodol. From the result, the DSB/SSB was higher in the build-up and within the Lipiodol than without the Lipiodol. The DSB yield is increased, which indicates the enhancement of the biological effect. This result was agreement with the previous studies in the point of that the radiosensitization considered with the biological effect was greater than the physical dose enhancement by the simulation [45–48]. In the build-up region and within the Lipiodol region, the scattered electrons with lower energy from the Lipiodol were increased. The lower energies are absorbed in the Lipiodol; thus the average energy is increased in the build-down region. The higher average energy decreases the DSB yield and the RBE. The average energy of the incident and scattered photon and electrons affects the DSB yield and the RBE.

In the comparison of the FF and FFF beams, the FFF beam has a larger biological effect than FF beam for both Lipiodol and water. The FFF beam contains more lower photon and electrons than FF beam [21]. Suneil et al. examined in vitro radiosensitization by GNP in MDA-MB-231 cells for 6 MV and 15 MV photon energies [47]. The sensitizer enhancement ratio with and without the GNP was 1.29 for 6 MV X-rays and 1.16 for 15 MV X-rays. Rahman et al. reported on the dose enhancement factors at 90% cell survival, which was 2.9 for 6MV X-rays and 3.7 for 12 MV at 0.5 mmol of GNPs [49]. These results indicate that the lower photon energy causes more radiosensitization. Matsuya et al. reported that the maximum of the yield of DSB occurred at 300 eV of the electron energy [27]. In the previous study, we showed that FFF beam contained more photons and electrons with energies mostly at 300 eV [20]. The lower photon beam increases the DSB yield and RBE. Therefore, the RBE_{DSB} with FFF beam was higher in the build-up region and within the Lipiodol than that with FF beam.

In the clinical liver SBRT, Lipiodol has been used as an embolic agent and for tumor seeking in

trans-arterial chemoembolization (TACE). Lipiodol remains in the tumor during radiotherapy treatment. The Lipiodol has a benefit to enhance radiobiological effect in the tumor intensively. Moreover, the radiobiological effect can be increased more by the irradiation in the tumor with the Lipiodol with FFF beam. The average energy of the incident and scattered photon and electrons affects the DSB yield and the RBE.

There is a limitation in the current study. The current study was performed with the simulation. The maximum enhancement of the RBE_{DSB} was 4.2% for 6MVX FFF beam. Further study to evaluate the effects of radiobiology by comparing the result in vivo or vitro and simulation is needed.

Conclusions

The current study simulated the DNA strand break except for the physical dose difference. The result suggest that DNA damage increased within the Lipiodol and the build-up region. Additionally, the lower and FFF beam occurred the higher biological effect. It might be benefit for the clinical treatment in the point that the Lipiodol enhance the DNA damage for the tumor locally.

Data availability

The data that support the findings of this study are available from the corresponding author upon reasonable request.

Conflict of interest

None declared.

Funding

None declared.

References

1. Friedland W, Kundrať P. Stochastic multi-scale modeling of biological effects induced by ionizing radiation. In: El Naqa I. ed. *A Guide to Outcome Modeling in Radiotherapy and Oncology: Listening to the Data*. CRC Press, Boca Raton 2018.
2. Nikjoo H, Uehara S, Emfietzoglou D. Interaction of photons with matter. In: Nikjoo H, Uehara S, Emfietzoglou D. ed. *Interaction of radiation with matter*. CRC Press, Routledge 2012: 89–102.
3. Wouters BG, Begg AC. Irradiation-induced damage and the DNA damage response. In: Joiner M, van der Kogel AJ. ed. *Basic Clinical Radiobiology*. Taylor & Francis, Routledge 2009: 11–26.

4. Famulari G, Pater P, Enger SA. Microdosimetry calculations for monoenergetic electrons using Geant4-DNA combined with a weighted track sampling algorithm. *Phys Med Biol*. 2017; 62(13): 5495–5508, doi: [10.1088/1361-6560/aa71f6](https://doi.org/10.1088/1361-6560/aa71f6), indexed in Pubmed: [28486214](https://pubmed.ncbi.nlm.nih.gov/28486214/).
5. Friedland W, Dingfelder M, Kundrát P, et al. Track structures, DNA targets and radiation effects in the biophysical Monte Carlo simulation code PARTRAC. *Mutat Res*. 2011; 711(1-2): 28–40, doi: [10.1016/j.mrfmmm.2011.01.003](https://doi.org/10.1016/j.mrfmmm.2011.01.003), indexed in Pubmed: [21281649](https://pubmed.ncbi.nlm.nih.gov/21281649/).
6. Liamsuwan T, Emfietzoglou D, Uehara S, et al. Microdosimetry of low-energy electrons. *Int J Radiat Biol*. 2012; 88(12): 899–907, doi: [10.3109/09553002.2012.699136](https://doi.org/10.3109/09553002.2012.699136), indexed in Pubmed: [22668077](https://pubmed.ncbi.nlm.nih.gov/22668077/).
7. Incerti S, Baldacchino G, Bernal M, et al. The Geant4-DNA project. *Int J Mod Simul Sci Comput*. 2012; 01(02): 157–178, doi: [10.1142/s1793962310000122](https://doi.org/10.1142/s1793962310000122).
8. Kai T, Yokoya A, Ukai M, et al. Cross sections, stopping powers, and energy loss rates for rotational and phonon excitation processes in liquid water by electron impact. *Radiat Phys Chem*. 2015; 108: 13–17, doi: [10.1016/j.radphyschem.2014.11.008](https://doi.org/10.1016/j.radphyschem.2014.11.008).
9. Kai T, Yokoya A, Ukai M, et al. Deceleration processes of secondary electrons produced by a high-energy Auger electron in a biological context. *Int J Radiat Biol*. 2016; 92(11): 654–659, doi: [10.1080/09553002.2016.1195933](https://doi.org/10.1080/09553002.2016.1195933), indexed in Pubmed: [27332896](https://pubmed.ncbi.nlm.nih.gov/27332896/).
10. Kai T, Yokoya A, Ukai M, et al. Thermal equilibrium and prehydration processes of electrons injected into liquid water calculated by dynamic Monte Carlo method. *Radiat Phys Chem*. 2015; 115: 1–5, doi: [10.1016/j.radphyschem.2015.05.021](https://doi.org/10.1016/j.radphyschem.2015.05.021).
11. Bedford JS. Sublethal damage, potentially lethal damage, and chromosomal aberrations in mammalian cells exposed to ionizing radiations. *Int J Radiat Oncol Biol Phys*. 1991; 21(6): 1457–1469, doi: [10.1016/0360-3016\(91\)90320-4](https://doi.org/10.1016/0360-3016(91)90320-4), indexed in Pubmed: [1938554](https://pubmed.ncbi.nlm.nih.gov/1938554/).
12. Sachs RK, Hahnfeldt P, Brenner DJ. The link between low-LET dose-response relations and the underlying kinetics of damage production/repair/misrepair. *Int J Radiat Biol*. 1997; 72(4): 351–374, doi: [10.1080/095530097143149](https://doi.org/10.1080/095530097143149), indexed in Pubmed: [9343102](https://pubmed.ncbi.nlm.nih.gov/9343102/).
13. Brenner DJ, Hlatky LR, Hahnfeldt PJ, et al. The linear-quadratic model and most other common radiobiological models result in similar predictions of time-dose relationships. *Radiat Res*. 1998; 150(1): 83–91, indexed in Pubmed: [9650605](https://pubmed.ncbi.nlm.nih.gov/9650605/).
14. Ando K, Koike S, Nojima K, et al. Mouse skin reactions following fractionated irradiation with carbon ions. *Int J Radiat Biol*. 1998; 74(1): 129–138, doi: [10.1080/095530098141799](https://doi.org/10.1080/095530098141799), indexed in Pubmed: [9687982](https://pubmed.ncbi.nlm.nih.gov/9687982/).
15. Hawkins RB. A statistical theory of cell killing by radiation of varying linear energy transfer. *Radiat Res*. 1994; 140(3): 366–374, indexed in Pubmed: [7972689](https://pubmed.ncbi.nlm.nih.gov/7972689/).
16. Kawahara D, Nakano H, Ozawa S, et al. Relative biological effectiveness study of Lipiodol based on microdosimetric-kinetic model. *Phys Med*. 2018; 46: 89–95, doi: [10.1016/j.ejmp.2018.01.018](https://doi.org/10.1016/j.ejmp.2018.01.018), indexed in Pubmed: [29519415](https://pubmed.ncbi.nlm.nih.gov/29519415/).
17. Sato T, Kase Y, Watanabe R, et al. Biological dose estimation for charged-particle therapy using an improved PHITS code coupled with a microdosimetric kinetic model. *Radiat Res*. 2009; 171(1): 107–117, doi: [10.1667/RR1510.1](https://doi.org/10.1667/RR1510.1), indexed in Pubmed: [19138056](https://pubmed.ncbi.nlm.nih.gov/19138056/).
18. Sato T, Iwamoto Y, Hashimoto S, et al. Features of Particle and Heavy Ion Transport code System (PHITS) version 3.02. *J Nucl Sci Technol*. 2018; 55(6): 684–690, doi: [10.1080/00223131.2017.1419890](https://doi.org/10.1080/00223131.2017.1419890).
19. Kawahara D, Ozawa S, Saito A, et al. Dosimetric impact of Lipiodol in stereotactic body radiation therapy on liver after trans-arterial chemoembolization. *Med Phys*. 2017; 44(1): 342–348, doi: [10.1002/mp.12028](https://doi.org/10.1002/mp.12028), indexed in Pubmed: [28102954](https://pubmed.ncbi.nlm.nih.gov/28102954/).
20. Kawahara D, Ozawa S, Saito A, et al. Energy spectrum and dose enhancement due to the depth of the Lipiodol position using flattened and unflattened beams. *Rep Pract Oncol Radiother*. 2018; 23(1): 50–56, doi: [10.1016/j.rpor.2017.12.004](https://doi.org/10.1016/j.rpor.2017.12.004), indexed in Pubmed: [29348734](https://pubmed.ncbi.nlm.nih.gov/29348734/).
21. Kawahara D, Ozawa S, Kimura T, et al. Photon and electron backscatter dose and energy spectrum analysis around Lipiodol using flattened and unflattened beams. *J Appl Clin Med Phys*. 2019; 20(6): 178–183, doi: [10.1002/acm2.12560](https://doi.org/10.1002/acm2.12560), indexed in Pubmed: [30884060](https://pubmed.ncbi.nlm.nih.gov/30884060/).
22. Farman AG, Sharma S, George DI, et al. Backscattering from dental restorations and splint materials during therapeutic radiation. *Radiology*. 1985; 156(2): 523–526, doi: [10.1148/radiology.156.2.4011918](https://doi.org/10.1148/radiology.156.2.4011918), indexed in Pubmed: [4011918](https://pubmed.ncbi.nlm.nih.gov/4011918/).
23. Nadrowitz R, Feyerabend T. Backscatter dose from metallic materials due to obliquely incident high-energy photon beams. *Med Phys*. 2001; 28(6): 959–965, doi: [10.1118/1.1366664](https://doi.org/10.1118/1.1366664), indexed in Pubmed: [11439492](https://pubmed.ncbi.nlm.nih.gov/11439492/).
24. Cashmore J. Surface dose variations in 6 and 10 MV flattened and flattening filter-free (FFF) photon beams. *J Appl Clin Med Phys*. 2016; 17(5): 293–307, doi: [10.1120/jacmp.v17i5.6284](https://doi.org/10.1120/jacmp.v17i5.6284), indexed in Pubmed: [27685127](https://pubmed.ncbi.nlm.nih.gov/27685127/).
25. Storm L, Israel H. Photon cross sections from 1 keV to 100 MeV for elements Z=1 to Z=100. *Atomic Data and Nuclear Data Tables*. 1970; 7(6): 565–681, doi: [10.1016/s0092-640x\(70\)80017-1](https://doi.org/10.1016/s0092-640x(70)80017-1).
26. Puchalska M, Sihver L. PHITS simulations of absorbed dose out-of-field and neutron energy spectra for ELEKTA SL25 medical linear accelerator. *Phys Med Biol*. 2015; 60(12): N261–N270, doi: [10.1088/0031-9155/60/12/N261](https://doi.org/10.1088/0031-9155/60/12/N261), indexed in Pubmed: [26057186](https://pubmed.ncbi.nlm.nih.gov/26057186/).
27. Matsuya Y, Kai T, Yoshii Y, et al. Modeling of yield estimation for DNA strand breaks based on Monte Carlo simulations of electron track structure in liquid water. *J Applied Phys*. 2019; 126(12): 124701, doi: [10.1063/1.5115519](https://doi.org/10.1063/1.5115519).
28. Matsuya Y, Ohtsubo Y, Tsutsumi K, et al. Quantitative estimation of DNA damage by photon irradiation based on the microdosimetric-kinetic model. *J Radiat Res*. 2014; 55(3): 484–493, doi: [10.1093/jrr/rrt222](https://doi.org/10.1093/jrr/rrt222), indexed in Pubmed: [24515253](https://pubmed.ncbi.nlm.nih.gov/24515253/).
29. Matsuya Y, Satou Y, Hamada N, et al. DNA damage induction during localized chronic exposure to an insoluble radioactive microparticle. *Sci Rep*. 2019; 9(1): 10365, doi: [10.1038/s41598-019-46874-6](https://doi.org/10.1038/s41598-019-46874-6), indexed in Pubmed: [31316118](https://pubmed.ncbi.nlm.nih.gov/31316118/).
30. Kinashi Y, Takahashi S, Kashino G, et al. DNA double-strand break induction in Ku80-deficient CHO cells following boron neutron capture reaction. *Radiat Oncol*. 2011; 6: 106, doi: [10.1186/1748-717X-6-106](https://doi.org/10.1186/1748-717X-6-106), indexed in Pubmed: [21888676](https://pubmed.ncbi.nlm.nih.gov/21888676/).
31. Kai T, Yokoya A, Ukai M, et al. A significant role of non-thermal equilibrated electrons in the formation of deleterious complex DNA damage. *Phys Chem Chem Phys*. 2018; 20(4): 2838–2844, doi: [10.1039/c7cp06903k](https://doi.org/10.1039/c7cp06903k), indexed in Pubmed: [29327017](https://pubmed.ncbi.nlm.nih.gov/29327017/).

32. Nikitaki Z, Nikolov V, Mavragani IV, et al. Measurement of complex DNA damage induction and repair in human cellular systems after exposure to ionizing radiations of varying linear energy transfer (LET). *Free Radic Res.* 2016; 50(sup1): S64–S78, doi: [10.1080/10715762.2016.123248](https://doi.org/10.1080/10715762.2016.123248), indexed in Pubmed: [27593437](https://pubmed.ncbi.nlm.nih.gov/27593437/).
33. Date H, Yoshii Y, Sutherland KL. Nanometer site analysis of electron tracks and dose localization in bio-cells exposed to X-ray irradiation. *Nucl Instr Methods Phys Res.* 2009; 267(7): 1135–1138, doi: [10.1016/j.nimb.2009.02.048](https://doi.org/10.1016/j.nimb.2009.02.048).
34. Yoshii Y, Sasaki K, Matsuya Y, et al. Cluster analysis for the probability of DSB site induced by electron tracks. *Nucl Instr Methods Phys Res.* 2015; 350: 55–59, doi: [10.1016/j.nimb.2015.03.025](https://doi.org/10.1016/j.nimb.2015.03.025).
35. Ashley JC. Stopping Power of Liquid Water for Low-Energy Electrons. *Radiat Res.* 1982; 89(1): 25, doi: [10.2307/3575681](https://doi.org/10.2307/3575681).
36. Herold DM, Das IJ, Stobbe CC, et al. Gold microspheres: a selective technique for producing biologically effective dose enhancement. *Int J Radiat Biol.* 2000; 76(10): 1357–1364, doi: [10.1080/09553000050151637](https://doi.org/10.1080/09553000050151637), indexed in Pubmed: [11057744](https://pubmed.ncbi.nlm.nih.gov/11057744/).
37. Regulla D, Schmid E, Friedland W, et al. Enhanced Values of the RBE and H Ratio for Cytogenetic Effects Induced by Secondary Electrons from an X-Irradiated Gold Surface. *Radiat Res.* 2002; 158(4): 505–515, doi: [10.1667/0033-7587\(2002\)158\[0505:evotra\]2.0.co;2](https://doi.org/10.1667/0033-7587(2002)158[0505:evotra]2.0.co;2).
38. Luchette M, Korideck H, Makrigiorgos M, et al. Radiation dose enhancement of gadolinium-based AGuIX nanoparticles on HeLa cells. *Nanomedicine.* 2014; 10(8): 1751–1755, doi: [10.1016/j.nano.2014.06.004](https://doi.org/10.1016/j.nano.2014.06.004), indexed in Pubmed: [24941464](https://pubmed.ncbi.nlm.nih.gov/24941464/).
39. Robar JL, Riccio SA, Martin MA. Tumour dose enhancement using modified megavoltage photon beams and contrast media. *Phys Med Biol.* 2002; 47(14): 2433–2449, doi: [10.1088/0031-9155/47/14/305](https://doi.org/10.1088/0031-9155/47/14/305), indexed in Pubmed: [12171332](https://pubmed.ncbi.nlm.nih.gov/12171332/).
40. Cui L, Tse K, Zahedi P, et al. Hypoxia and cellular localization influence the radiosensitizing effect of gold nanoparticles (AuNPs) in breast cancer cells. *Radiat Res.* 2014; 182(5): 475–488, doi: [10.1667/RR13642.1](https://doi.org/10.1667/RR13642.1), indexed in Pubmed: [25361396](https://pubmed.ncbi.nlm.nih.gov/25361396/).
41. Geng F, Song K, Xing JZ, et al. Thio-glucose bound gold nanoparticles enhance radio-cytotoxic targeting of ovarian cancer. *Nanotechnology.* 2011; 22(28): 285101, doi: [10.1088/0957-4484/22/28/285101](https://doi.org/10.1088/0957-4484/22/28/285101), indexed in Pubmed: [21654036](https://pubmed.ncbi.nlm.nih.gov/21654036/).
42. Liu Y, Liu Xi, Jin X, et al. The dependence of radiation enhancement effect on the concentration of gold nanoparticles exposed to low- and high-LET radiations. *Phys Med.* 2015; 31(3): 210–218, doi: [10.1016/j.ejmp.2015.01.006](https://doi.org/10.1016/j.ejmp.2015.01.006), indexed in Pubmed: [25651760](https://pubmed.ncbi.nlm.nih.gov/25651760/).
43. Wolfe T, Chatterjee D, Lee J, et al. Targeted gold nanoparticles enhance sensitization of prostate tumors to megavoltage radiation therapy in vivo. *Nanomedicine.* 2015; 11(5): 1277–1283, doi: [10.1016/j.nano.2014.12.016](https://doi.org/10.1016/j.nano.2014.12.016), indexed in Pubmed: [25652893](https://pubmed.ncbi.nlm.nih.gov/25652893/).
44. Rosa S, Connolly C, Schettino G, et al. Biological mechanisms of gold nanoparticle radiosensitization. *Cancer Nanotechnol.* 2017; 8(1): 2, doi: [10.1186/s12645-017-0026-0](https://doi.org/10.1186/s12645-017-0026-0), indexed in Pubmed: [28217176](https://pubmed.ncbi.nlm.nih.gov/28217176/).
45. Butterworth KT, McMahon SJ, Currell FJ, et al. Physical basis and biological mechanisms of gold nanoparticle radiosensitization. *Nanoscale.* 2012; 4(16): 4830–4838, doi: [10.1039/c2nr31227a](https://doi.org/10.1039/c2nr31227a), indexed in Pubmed: [22767423](https://pubmed.ncbi.nlm.nih.gov/22767423/).
46. Ionita P, Gilbert BC, Chechik V. Radical mechanism of a place-exchange reaction of au nanoparticles. *Angew Chem Int Ed Engl.* 2005; 44(24): 3720–3722, doi: [10.1002/anie.200500518](https://doi.org/10.1002/anie.200500518), indexed in Pubmed: [15880720](https://pubmed.ncbi.nlm.nih.gov/15880720/).
47. Jain S, Coulter JA, Hounsell AR, et al. Cell-specific radiosensitization by gold nanoparticles at megavoltage radiation energies. *Int J Radiat Oncol Biol Phys.* 2011; 79(2): 531–539, doi: [10.1016/j.ijrobp.2010.08.044](https://doi.org/10.1016/j.ijrobp.2010.08.044), indexed in Pubmed: [21095075](https://pubmed.ncbi.nlm.nih.gov/21095075/).
48. Chithrani DB, Jelveh S, Jalali F, et al. Gold nanoparticles as radiation sensitizers in cancer therapy. *Radiat Res.* 2010; 173(6): 719–728, doi: [10.1667/RR1984.1](https://doi.org/10.1667/RR1984.1), indexed in Pubmed: [20518651](https://pubmed.ncbi.nlm.nih.gov/20518651/).
49. Rahman WN, Bishara N, Ackerly T, et al. Enhancement of radiation effects by gold nanoparticles for superficial radiation therapy. *Nanomedicine.* 2009; 5(2): 136–142, doi: [10.1016/j.nano.2009.01.014](https://doi.org/10.1016/j.nano.2009.01.014), indexed in Pubmed: [19480049](https://pubmed.ncbi.nlm.nih.gov/19480049/).